Detection of In-Flight Propeller-Induced Structure-Borne Noise

J. F. Unruh*
Southwest Research Institute, San Antonio, Texas

A potentially important source of structure-borne interior noise transmission in advanced turboprop aircraft is the impingement of the propeller wake/vortex on downstream aerodynamic surfaces. It can be safely assumed that this potential source of interior noise may well adversely affect achievable interior noise levels unless noise control measures are conscientiously incorporated into the aircraft design. Through the use of a laboratory-based test apparatus, techniques were developed to estimate the level of in-flight structure-borne noise transmission from combined frequency response function ground testing and in-flight structural response measurements. All phases of the procedure were simulated in the laboratory and the expected level of accuracy of the procedure is addressed.

Introduction

A MAJOR focus of interior noise control for twin-engine propeller aircraft has been the reduction of the propeller direct airborne component via improved sidewall treatments.[1-4] A majority of the research effort in this area has been aimed at the advanced high-speed turboprop aircraft wherein the direct airborne propeller-generated noise is quite intense and appears to be most critical for the success of this new generation aircraft.[5] Continued efforts to develop lightweight sidewall treatments are presently being pursued[6] and, coupled with the development of improved high-speed, low-noise propeller designs,[7] the direct airborne sidewall transmission problem may well be resolved in the near future. However, the potential for other sources and transmission paths governing the interior noise levels is quite high, based on most recent discoveries and historical data.

Historically speaking, interior noise levels of propeller-driven aircraft are much higher than the acceptable levels of present-day turbofan aircraft, even after apparently ample application of noise control measures. Engine vibration-induced, structure-borne interior noise transmission has been shown to be equal to or greater than the direct airborne noise transmission levels in a single-engine, propeller-driven aircraft.[8] The potential for engine vibration as a source of structure-borne interior noise in twin-engine aircraft has not been thoroughly investigated; nevertheless, adequate procedures for engine vibration isolation system evaluation have been developed.[9-10]

A potentially more important source of structure-borne interior noise transmission is provided by the interaction of the propeller wake and aircraft wing structure. The wing surface downstream of the propeller may experience significant aerodynamically induced, fluctuating pressures due to the propeller wake, especially from the tip vortex.[11] Extensive ground tests of a Twin Otter aircraft revealed that the propeller wake and tip vortex interaction with the wing surface was the major source of interior noise for the aircraft at 50% or greater engine torque.[12] The interior noise spectra were dominated by contributions at the propeller blade passage frequency and its harmonics.

The expected levels of propeller wake/vortex-induced, structure-borne noise transmission in an advanced turboprop aircraft is not known, nor can it be determined with present-day technology. It can only be safely assumed that this source of interior noise may well adversely affect achievable interior levels unless several noise control measures are conscientiously incorporated into the aircraft design. Thus, the research community must provide the airframe designer with structure-borne noise prediction capabilities, control methodology, and detection techniques.

Early in 1985, a research program, supported by NASA Langley Research Center, was undertaken to develop an understanding of the propeller wake/vortex-induced, structure-borne noise transmission phenomenon. The program approach to achieve this objective was to develop a laboratory-based test apparatus that would allow the study and development of reliable structure-borne noise detection techniques and the systematic evaluation of potential noise control measures. The design, construction, and evaluation of the laboratory facility is complete and is briefly described in this paper. Work on developing reliable structure-borne noise detection techniques has been carried out as reported herein and the evaluation of noise control measures is presently under way.

In the text to follow, the major components of the test apparatus are described and its capabilities documented. Thereafter, the procedures developed to detect in-flight structure-borne noise transmission due to propeller wake/vortex excitation is described, along with data analysis procedures. Typical results are then given, as well as the expected level of accuracy of the procedures.

Test Apparatus

The principal approach to the test apparatus design was to provide a physical means of separating the airborne and structure-borne noise components so that the structure-borne noise transmission response could be studied directly without airborne noise contamination. The primary components of the test apparatus, i.e., the wing, fuselage, propeller source, and acoustic shield (with enclosed fuselage), are shown in Fig. 1.

The wing structure is a 31.0 in. constant chord NACA 0012 section airfoil with an exposed span of 80 in. The structure is of conventional sheet metal and rivet construction with 0.040 in. skin with ribs on 16.0 in. centers. The wing front and rear spars, at 29 and 75% chord, extend an additional length of 13.5 in. beyond the skin surface (see Fig. 2) to accommodate penetration through the fuselage acoustic shield and attachment to the fuselage. The wing structure weighs a total of 29.55 lb.

The wing-to-fuselage attachment structure is shown in Figs. 2 and 3. Spherical bearings are used at each of the three attachment points to eliminate local moment transfer; only shear transfer is allowed. Overall wing moments are reacted by lateral differential shear in the front spar only. This physical

Received Nov. 11, 1986; revision received Jan. 29, 1987.

*Staff Engineer, Department of Engineering Mechanics, Division of Engineering and Materials Sciences. Senior Member AIAA.

arrangement confines the structure-borne noise transmission path to well-defined motions at the wing/fuselage attach points. Both the front and rear spar fuselage-to-wing attachments are directly secured to the fuselage floor beams and ring frames; see Fig. 4. Additional floor beam cap stiffeners were used to carry the wing loads across the fuselage.

The fuselage structure is a 72 in. long and 40 in. diameter cylinder with 0.032 in. thick skin. The cylinder is stiffened by 18 evenly spaced stringers. The stringers are riveted to the cylinder skin and pass through eight internal ring frames spaced on 8.0 in. centers. A schematic of the fuselage cross section is shown in Fig. 5. The floor of the cylinder, 0.032 in. thick, is supported on continuous floor beams, extending across the ring frames (see Fig. 4) at a distance of 11.0 in. from the cylinder center. Two longitudinal floor beams extend the length of the fuselage. The fuselage floor is bolted to the floor support beams and to the cyclinder outer skin. The fuselage endcaps are ½ in. thick solid aluminum plate.

The fuselage interior trim consists of a ½ in. thick fiberglass blanket with a 0.002 in. thick vinyl film facing on each endcap. Four layers of the same material completely line the walls of the cyclinder, including the area below the floor. The cabin sidewall area is finished with a sheet of epoxy/fiberglass material, 0.032 in. thick. An additional 0.032 in. sheet of vinyl is used in a 120 deg sector as a headliner trim. The total weight of the fuselage is approximately 241 lb, with 125 lb being the solid aluminum endcaps.

In order to minimize the transmission of airborne propeller noise into the fuselage cabin, a 5½ in. thick, 54 in. i.d., 7 ft long concrete shield weighing 7000 lb was used to house the fuselage; see Fig. 6. The acoustic shield has 4½ in. thick wooden removable endcaps for access. The endcaps bolt to the acoustic shield using a rubber seal to prevent acoustic leakage. The acoustic shield and endcaps were fitted with 2.0 in. thick fiberglass, canvas-faced blankets to reduce reverberant sound buildup in the air gap between the shield and fuselage (see Fig. 6).

The wing penetrates the acoustic shield at only two relatively small areas, sufficient to clear the extended front and rear spars. An acoustic seal, consisting of a molded base to fit the shield and wing contours, and a pair of 3 in. thick adjustable blocks, also contoured to the wing cross-sectional profile, are used to reduce direct airborne noise radiation. The air gap between the wing and the seal blocks is set to approximately 3/16 in. all the way around the wing surface and extends into the seal base to a depth of approximately 4½ in.,

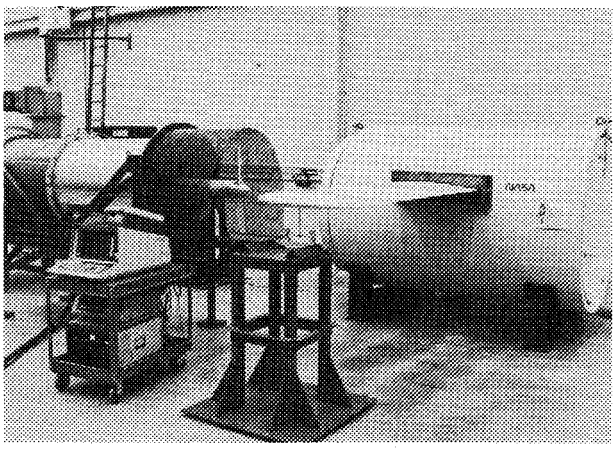

Fig. 1 Test apparatus overview.

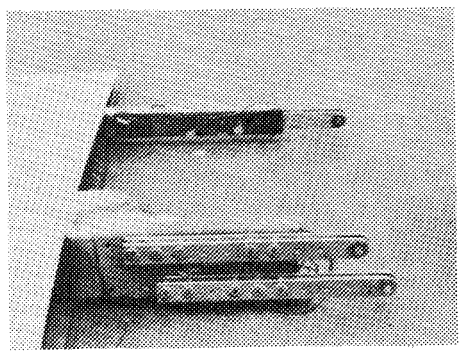

Fig. 2 Wing attachment fittings.

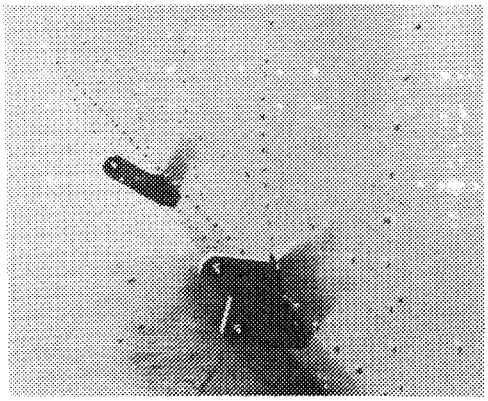

Fig. 3 Wing-to-fuselage front and rear carrythrough attachments.

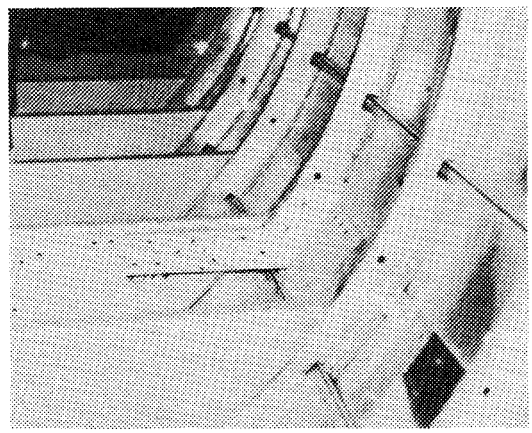

Fig. 4 Wing front spar attachment structure.

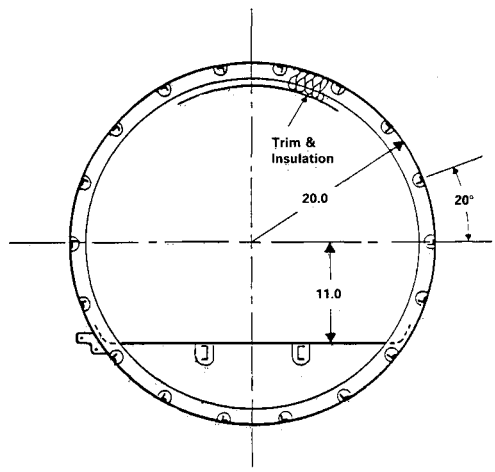

Fig. 5 Fuselage structural details.

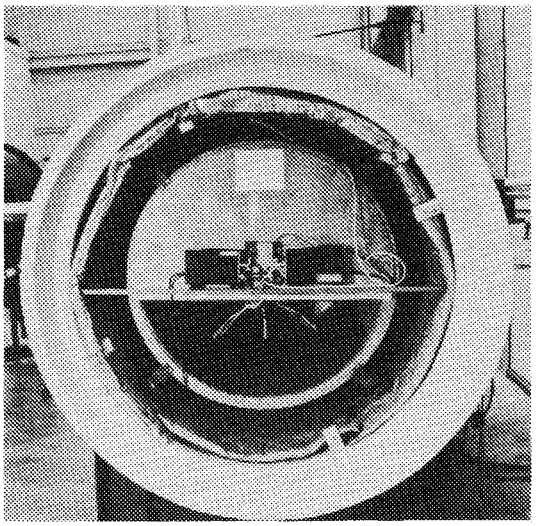

Fig. 6 Fuselage in acoustic shield.

after which an abrupt transmission to the spar penetration holes occurs. The wing acoustic seal thus provides a rather torturous sound propagation path, which is desired for high transmission loss. In order to maintain the 3/16 in. gap during propeller excitation, the wing tip is fitted with a ground spring to reduce low-frequency wing buffeting.

The fuselage is supported on either end via four equally spaced elastomeric vibration supports attached to the acoustic shield. The isolators were chosen to provide a fuselage/wing support frequency below 15 Hz to prevent flanking vibration through the supports into the fuselage. A more detailed description of the test apparatus is given in Ref. 13.

The propeller source is a 23 in. diameter propeller with a modified Clark-Y section and nearly constant 3⅛ in. chord. The propeller is powered by an 18 hp hydraulic motor with a maximum speed of 6000 rpm. A low-pressure, nine-blade vane axial fan powered by a 20 hp electric motor provides a 33 in. diameter, 70 ft/s inlet flow to the propeller to simulate forward flight. Flow swirl in the fan is reduced via 12 stationary turning vanes and 2 downstream 3.0 in. thick sections of ½ in. hexagonal honeycomb. The propeller source and vane axial fan are vibration isolated and mounted to a common base. The common base is on telescoping legs and can be readily positioned.

The maximum speed of the propeller is 5700 rpm, requiring approximately 13.5 hp and producing a maximum thrust of 30 lb. The propeller speed can be set and held to within ±5 rpm. The propeller produces a high level of airborne noise, as can be seen in the spectra shown in Fig. 7. The two-blade propeller fundamental, at a speed of 5100 rpm, occurs at 170 Hz. The first five propeller tones are readily seen in both the source and fuselage interior spectra. Several other distinct periodic components are present in the source spectra, which can be attributed to the propeller inlet air source that operates at 1750 rpm. The axial fan has nine blades, giving rise to a 262.5 Hz fundamental with 525 and 787.5 Hz harmonics. The periodic components near 600 and 800 Hz are attributed to the gearing of the hydraulic motor and hydraulic power supply. The propeller harmonics are easily identified in the interior microphone spectra.

The performance of the acoustic seal at the wing/fuselage interface was a major concern in the development of the test apparatus. Its performance was evaluated by subjecting the seal to direct airborne noise excitation via an acoustic speaker. An external reference microphone was located near the seal gap and a second microphone was placed just inside of the acoustic shield near the wing front spar where transmission from the acoustic seal leakage would be at maximum. The interior spectra exhibited a 20 dB, or greater, SPL transmission

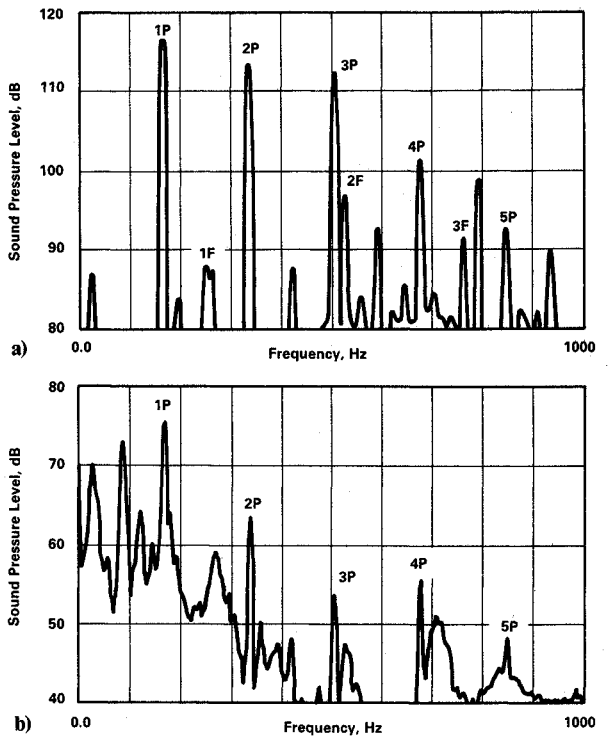

Fig. 7 Typical propeller spectra at 5100 rpm: a) source, b) fuselage interior.

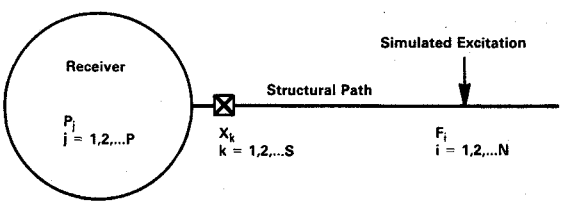

Fig. 8 Test setup schematic.

loss throughout the frequency range of interest (50–1000 Hz). When the 3/16 in. gap was closed with a high-density putty, only marginal increases in transmission loss occurred and, thus, no further practical improvement in seal design appeared to be necessary.

To determine the dynamic range of the test apparatus for structure-borne noise control measure development/evaluation, test runs were carried out for wing-attached and wing-detached configurations. In the wing-detached configuration, the wing was placed into the acoustic shield in the normal attached configuration; however, support was provided by small wooden wedges placed in the acoustic seal gap. The wing front and rear spar fuselage attachment bolts were not installed and contact between the two structures was not allowed. The wooden wedges introduced less than a 5% blockage of the acoustic seal. The major effect was to cut the wing vibration transmission path and, hence, structure-borne noise transmission. Data with the wing attached and detached were acquired at fixed propeller speeds of 3450, 4260, 4980, and 5700 rpm. Interior sound pressure levels were acquired at 12 interior microphone locations. Spatial average interior noise levels were computed from the interior microphones. The resulting data are presented in Table 1. As can be seen, sufficient dynamic range exists throughout the higher propeller speeds for structure-borne noise detection procedures and control measure development.

Test Procedure

The test procedure for detection of in-flight propeller-induced, structure-borne noise is most easily described with reference to the schematic of Fig. 8. The structural path, being the wing structure, is excited with simulated forces F_i at N locations in the area of the propeller wake and S structural response measurements X_k are acquired, along with P interior microphone responses P_j. During ground test measurements, the pressure response to input force,

$$HPF(\omega)_{ji} = P(\omega)_j / F(\omega)_i \quad (1)$$

frequency response functions (FRF's) are computed, along with structural response to input force FRF's.

$$HXF(\omega)_{ki} = X(\omega)_k / F(\omega)_i \quad (2)$$

The pressure response to structural response FRF's are then computed as

$$HPX(\omega)_{ijk} = HPF(\omega)_{ji} / HXF(\omega)_{ki} \quad (3)$$

During flight test, the structural responses $\bar{X}(\omega)_k$ are acquired and estimates of interior structure-borne noise levels are computed from the ground-based FRF's as

$$\bar{P}(\omega)_{ijk} = HPX(\omega)_{ijk} * \bar{X}(\omega)_k \quad (4)$$

A variation in the computed interior levels occurs from the multiple simulated excitation, multiple structural response measurements, and multiple microphone locations within the receiving cabin.

This procedure appears straightforward; however, upon application several questions arise: 1) which structural response parameters, acceleration, strain, etc., should be utilized; 2) at what structural locations for optimum results; and 3) what type of simulated force excitation should be used in the FRF acquisition? The propeller-induced, structure-borne noise test apparatus was utilized to answer several of these questions. The apparatus was employed, as shown in Fig. 1, to record frequency response function data and propeller-induced structure-borne noise level data. The fuselage structure was then removed from the acoustic shield and propeller excitation was used to simulate in-flight conditions wherein both

Table 1 Test apparatus dynamic range

Configuration	Spatial average noise level, dB 3450 rpm	4260 rpm	4980 rpm	5700 rpm
1st propeller tone				
Wing attached	54.3	62.9	82.1	91.7
Wing detached	41.9	55.8	65.6	63.5
ΔdB	12.4	7.1	16.5	28.2
2nd propeller tone				
Wing attached	57.9	45.4	59.4	69.9
Wing detached	49.1	44.0	40.8	48.5
ΔdB	8.8	1.4	18.6	21.4

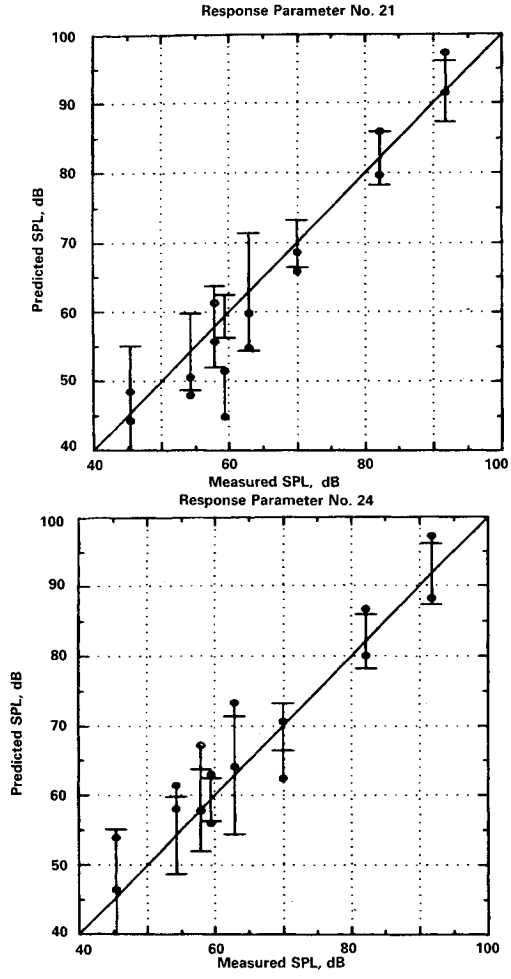

Fig. 9 Predicted vs measured SBN, wing front spar lateral response: a) strain, b) acceleration.

Table 2 Typical response parameter sensitivity, first propeller tone

Response parameter	Location	Sensitivity dB/unit response 3450 rpm, 115 Hz Mean	σ	4260 rpm, 142 Hz Mean	σ	4980 rpm, 166 Hz Mean	σ	5700 rpm, 190 Mean	σ
Lat. strain/wing root,									
Fwd. spar, lower flange	21	69.7	1.3	72.4	2.5	84.8	3.1	87.3	2.9
Fwd. spar, upper flange	22	70.1	1.3	72.8	2.5	85.2	3.1	87.8	2.9
Rear spar, web center	23	68.0	1.3	70.7	2.5	83.1	3.1	85.7	2.9
Lat. accel./wing root,									
Fwd. spar, lower flange	24	105.3	1.7	100.0	4.6	100.8	3.3	104.1	4.5
Fwd. spar, upper flange	25	102.8	2.6	98.0	4.6	100.1	3.5	104.7	4.9
Rear spar, web center	26	106.1	2.4	98.7	4.5	101.3	3.3	104.6	5.8
Vert. accel./wing root,									
Fwd. spar, lower flange	27	68.5	1.4	64.7	5.3	75.9	4.2	74.9	5.5
Fwd. spar, upper flange	28	67.8	1.3	64.3	5.3	76.0	4.1	74.8	5.3
Rear spar, web center	29	66.9	2.0	72.7	5.3	79.1	4.8	65.2	7.4
Vert. accel./cabin floor,									
Hard structure	30	95.2	1.4	102.0	2.2	101.7	2.1	112.4	2.9
Panel structure	31	101.2	1.4	108.0	2.2	107.7	2.1	118.4	2.9

structure-borne and direct propeller airborne noise excitation of the fuselage occurs.

Data Acquisition

Hammer impulse excitation was chosen for the simulated ground test frequency response function acquisition. The impulse technique produces a broadband input and, within five to seven sample averages, produces highly repeatable results. While the signal-to-noise ratios were not as high as would be possible with single-frequency sinusoidal excitation, they nevertheless appeared adequate for the initial evaluation. Six excitation locations were used on the wing hard structure in the propeller wake area. The wing front and rear spars, near the root (see Fig. 2), were instrumented with accelerometers and strain gages. Strain gages were used to record lateral strain in the front spar upper and lower flanges and the rear spar center web areas. Lateral response accelerometers were also used in the same areas, along with a set of vertical response accelerometers. In addition to these nine structural response parameters denoted, respectively, as 21–29, two vertical response accelerometers were used in the cabin to record floor motion on a hard structure point (30) and at a panel center (31). Twelve microphone locations were used to record interior sound pressure level responses.

Frequency response function spectra were obtained in a frequency range of 0–750 Hz, with an analysis bandwidth of 1.875 Hz, using a commercially available spectrum analyzer linked to a minicomputer. The frequency range of primary interest was 115–590 Hz, which covers the first through third propeller tones in the propeller speed range of 3450–5700 rpm.

The 23 channels of response data were also recorded on an FM magnetic tape recorder during propeller excitation of the wing surface at set speeds of 3450, 4260, 4980, and 5700 rpm for both structure-borne noise transmission only and simulated in-flight excitation (fuselage exposed to propeller acoustic field).

Table 3 Correlation of predicted vs measured SBN and SBN excitation

Response parameter no.	Standard deviation of residuals, $\sigma_{Avg,SPL}$, dB R40	R50	R60
21	1.76	2.01	1.70
22	1.30	1.39	1.64
23	4.61	5.09	6.97
24	1.38	1.42	1.73
25	2.79	2.76	1.22
26	2.54	2.53	3.03
27	8.37	9.47	13.31
28	6.87	7.81	9.93
29	7.50	8.41	11.59
30	3.53	4.01	5.96
31	3.10	3.40	4.78

Table 4 Correlation of predicted vs measured SBN, in-flight simulation

Response parameter no.	Standard deviation of residuals, $\sigma_{Avg,SPL}$, dB R40	R50	R60
21	1.93	0.97	1.48
22	2.18	1.72	2.20
23	3.03	3.18	3.17
24	3.77	3.45	4.17
25	4.08	2.83	4.02
26	3.96	3.68	3.75
27	4.29	4.86	6.44
28	5.21	5.90	7.95
29	4.05	4.63	7.12
30	3.99	4.13	6.00
31	5.73	4.43	6.09

Data Analysis

The response ratios *HPF* and *HXF* were peak picked from the hammer impact frequency response function data at frequencies corresponding to the first three propeller tones at the four set propeller speeds. Typical spatial average response parameter sensitivities, i.e., the *HPX* ratio, are given in Table 2 for the first propeller tone. The standard deviation of the response parameter sensitivity is derived from the variation of response due to the 6 independent hammer excitations and the average of the 12 interior microphone responses making up the spatial average response. It is of interest to note that the sensitivities are rather uniform across groups of response parameters and even across the frequency spectrum. However, direct comparison of a strain parameter response in decibels per microstrain and an accelerometer response in decibels per unit gravity does not lend itself to useful interpretation. Recalling the definition of the response parameter ratio *HPX,* it is seen that a more sensitive structural response parameter corresponds to the smaller values listed in Table 2. The magnetically recorded propeller-running data were sample averaged and the spectra peak was chosen to produce corresponding tone structural responses for the structure-borne only and in-flight simulation configurations. These responses and the response parameter ratios were then combined to predict the level of expected structure-borne noise for the two propeller-running configurations.

Typical Results

A measure of the appropriateness of the proposed procedures is a direct comparison of the spatial average interior noise levels predicted from the simulated FRF ground test data and the measured structural responses during propeller excitation with the actual measured structure-borne noise levels. Typical correlation plots of such data are given in Fig. 9 for the wing front spar lateral strain and acceleration response

Table 5 Comparison of spatial average interior noise levels

Configuration	Response, dB: 3450 rpm, 345 Hz Mean	σ	4260 rpm, 426 Hz Mean	σ	4980 rpm, 498 Hz Mean	σ	5700 rpm, 570 Hz Mean	σ
First propeller tone								
Structure-borne only	54.3	5.5	62.9	8.5	82.1	3.8	91.7	4.4
In-flight simulation	67.1	5.7	74.0	5.8	88.0	3.1	94.8	4.9
Δdb	12.8		11.1		5.9		3.1	
Second propeller tone								
Structure-borne only	57.9	5.9	45.4	9.7	59.4	3.1	69.9	3.4
In-flight simulation	65.7	4.7	73.7	5.4	75.7	3.9	85.3	5.2
ΔdB	7.8		28.3		16.3		15.4	

parameters. The measured or "target" levels are plotted as the mean value $\pm 1\sigma$ (arising from a spatial average) as horizontal bars and the predicted levels plotted with $\pm 1\sigma$ as small circles. Only data for the first two propeller tones were employed in the data analysis, since the third propeller tone was generally near or into the apparatus noise floor. As can be seen by the data given in Fig. 9, the higher interior noise levels were well predicted using the proposed procedures.

A more quantitative interpretation of the accuracy of the predicted noise levels among the various structure response parameters is given by the standard deviation of the residual error between the target mean and predicted mean structure-borne noise level. Results of such analysis are given in Table 3, wherein the values listed under R40 consist of all data with measured interior levels above 40 dB, under R50 all data above 50 dB, etc. As can be seen, the front spar lateral strain and acceleration response parameters (Nos. 21, 22, 24, and 25) yield the best estimates of the "target" levels.

A similar analysis was carried out for the structural response data recorded during simulated in-flight operations. Predicted actual "target" structure-borne noise levels were compared and the standard deviation of the residual computed for each of the response parameters. Results of the analysis are given in Table 4. When comparing these results with those in Table 3, it can be seen that the wing front spar lateral strain response parameters were much less affected by the introduction of a high level of airborne noise radiation from the propeller than the acceleration response parameters, which showed both degradation and fortuitous improvement.

The significance of the accuracy obtained using the proposed procedures for predicting structure-borne noise levels during flight operations is best reviewed relative to the measured interior noise levels. A comparison of spatial average structure-borne and in-flight simulation interior noise levels recorded during the evaluation are given in Table 5 for the first two propeller tones. As can be seen, for several of the propeller tones, the in-flight simulation interior noise levels are measurably higher than the structure-borne only ones. At a value of 6.0 for ΔdB, the airborne noise transmission is equal to the structure-borne transmission; this is nearly the case for the first propeller tone at 4980 rpm. With the standard deviation of residuals (as given in Table 4) being a good estimate of the expected accuracy of the procedures, then, relative to the interior recorded noise levels (given in Table 5), the proposed procedures appear to be sufficiently accurate to indicate whether a structure-borne noise problem exists. If a structure-borne noise problem exists, the proposed procedures can also be used to evaluate the effectiveness of imposed control measures.

Conclusions and Recommendations

Through the use of a test procedure employing ground-based frequency response functions and in-flight structural response measurements, propeller-induced structure-borne noise levels can be predicted in the presence of high levels of airborne noise expected in flight.

Selection of appropriate structural response parameters is difficult; however, wing root strain appears to be most insensitive to airborne noise transmission and the major load-carrying structure, such as the wing front spar, appears to be an optimum location for such strain measurements.

It is believed that further improvement in source simulation during ground test evaluation will produce improved results. For the propeller source, a matched pair of shakers driven out of phase to produce a pure moment excitation will simulate the vortex action with the wing leading edge far better than the single-point force excitation. The use of a higher level of harmonic excitation will also greatly improve signal-to-noise ratios during frequency response function data acquisition. Based on this preliminary study, it is believed that the procedures can also be used to evaluate engine vibration transmission via excitation at the engine mounts.

Acknowledgments

The work reported herein was sponsored by NASA Langley Research Center under Contract NAS1-17921 and is greatly appreciated. The efforts of Mr. Frank R. Pitman during the facility setup and data acquisition phases of the work is gratefully acknowledged.

References

[1]Mixson, J. S. and Barton, C. K., "Investigation of Interior Noise in a Twin-Engine Light Aircraft," *Journal of Aircraft*, Vol. 15, April 1978, pp. 227-233.

[2]Barton, C. K. and Mixson, J. S., "Noise Transmission and Control for a Light, Twin-Engine Aircraft," AIAA Paper 80-1036, June 1980.

[3]Rennison, D. C., Wilby, J. F., March, A. H., and Wilby, E. G., "Interior Noise Control Prediction Study for High-Speed Propeller Driven Aircraft," NASA CR-159200, Sept. 1979.

[4]Revell, J. D., Balens, F. J., and Koval, L. R., "Analytical Study of Interior Noise Control by Fuselage Design Techniques on High-Speed, Propeller-Driven Aircraft," NASA CR-159222, July 1978.

[5]Dugan, J. F., Miller, B. A., Graber, E. J., and Sagersen, D. A., "The NASA High-Speed Turboprop Program," NASA TM 81561, Oct. 1980.

[6]Valcaitis, R. and Mixson, J. S., "Theoretical Design of Acoustic Treatment for Noise Control in a Turboprop Aircraft," *Journal of Aircraft*, Vol. 22, April 1985, pp. 303-310.

[7]Stefko, G. L., Bober, L. J., and Neumann, H. E., "New Test Techniques and Analytical Procedures for Understanding the Behavior of Advanced Propellers," SAE Paper 830729, April 1983.

[8]Unruh, J. F., Scheidt, D. C., and Pomerening, D. J., "Engine Induced Structure-Borne Noise in a General Aviation Aircraft," NASA CR-159099, Aug. 1979.

[9]Unruh, J. F. and Scheidt, D. C., "Engine Isolations for Structural-Borne Interior Noise Reduction in a General Aviation Aircraft," NASA CR-3427, May 1981.

[10]Unruh, J. F. and Scheidt, D. C., "Design and Test of Aircraft Engine Isolators for Reduced Interior Noise," NASA CR-166021, Dec. 1982.

[11]Miller, B. A., Dittman, J. H., and Jerachi, R. J., "The Propeller Tip Vortex—A Possible Contributor to Aircraft Cabin Noise," NASA TM 81768, April 1981.

[12]Metcalf, V. L. and Mayes, W. H., "Structure-borne Contribution to Interior Noise of Propeller Aircraft," SAE Paper 830735, April 1983.

[13]Unruh, J. F., "Propeller-Induced Structure-borne Noise: Laboratory-Based Test Apparatus," AIAA Paper 86-1938, July 1986.